Electronic Supplementary Material (ESI) for Dalton Transactions.
This journal is © The Royal Society of Chemistry 2018

A microstructured p-Si photo-cathode outcompetes Pt as a counter electrode to hematite in photo-electrochemical water-splitting

Anurag Kawde [1,2], Alagappan Annamalai [3], Anita Sellstedt[4], Pieter Glatzel [2], Thomas Wågberg[3], Johannes Messinger[1,5*]

[1] Umeå University, Department of Chemistry, Sweden

[2] European Synchrotron Radiation Facility (ESRF), Grenoble, France

[3] Umea University, Department of Physics, Sweden

[4]Umeå University, Department of Plant Physiology, Umeå Plant Science Centre (UPSC), Umeå, Sweden

[5]Molecular Biomimetics, Department of Chemistry, Ångström Laboratory, Uppsala University, Sweden

[*] Corresponding author. E-mail address: *johannes.messinger@kemi.uu.se*

S1.Experimental

S1.1 Semiconductor Photo-Electrodes (SPEs) Synthesis

The FTO/ α-Fe_2O_3 was prepared by hydrothermal growth of α-Fe_2O_3 nanorods on the FTO substrate as per the method described in ref[1]. In brief, 0.15 M ferric chloride and 1 M sodium nitrate solutions were adjusted to pH 1.2 by dropwise addition of HCl. The cleaned FTO substrates were immersed in this solution for 12 hours and kept in an autoclave at a constant temperature of 100^oC. The FTO/α-Fe_2O_3 electrodes were then rinsed with distilled water and ethanol followed by annealing at 800^oC. The p-Si microwires (MWs) was synthesised using a well-known metal assisted electroless etching method according to Peng et al.[2]. The as-synthesized p-Si MWs were then cleaned in a water diluted HNO_3 solution (1:1 by volume) followed by drying in air. Next, the as synthesised air-dried p-Si MWs was spin coated with the TiO_2 solution. The TiO_2 coated Si MWs were annealed at 380^oC in air followed by spin coating with NiO_x sol. The TiO_2 and NiO_x sol were prepared as per our previous study[3]. The resulting p-Si /TiO_2/NiO_x was then annealed at 380^oC and the samples were kept in a desiccator until used. The photo-electrochemical performance of the photoelectrodes was measured in 1 M NaOH (pH 13.8) under single and parallel-illumination mode.

S1.2 Photo-Electrochemical Characterization of SPEs

Three electrode photo-electrochemical measurements were performed in a conventional quartz electrochemical cell (from Pine Instruments) with Ag/AgCl as a reference electrode. The LSVs were performed using a Metrohm Autolab PGSTAT302N in the dark and in two different illumination modes. The illumination was achieved using a solar simulator (Newport- 94043A, equipped with 450W Xenon lamp and air-mass 1.5 filter) providing standard 1 sun condition. An additional light source from Thor Labs (neutral white- MNWHL4) was used to illuminate the p-Si/TiO_2/NiOx photocathode with a power density of 100 mW/cm^2, to achieve uniform illumination of both the electrodes in parallel illumination (PI)-mode. The LSVs obtained were converted into reversible hydrogen electrode potentials (V_{RHE}) using equation Eq. S1

$$\boldsymbol{V_{RHE} = V_{Ag/AgCl} + 0.1976 + (0.059 \times pH)} \qquad \textbf{Eq. S1}$$

The applied bias photon-to-current efficiency shown in Figure 3 (a) was deduced from the LSV curves shown in Figure 1 (a) using equation Eq.S2

$$\boldsymbol{ABPE}\ (\%) = \left[\frac{J\left(\frac{mA}{cm^2}\right) \times (1.23 - Vapp))}{P\left(\frac{mW}{cm^2}\right)}\right] \times 100 \qquad \textbf{Eq. S2}$$

The flat band potential (V_{fb}) as shown in Figure 3 (b) was calculated from the slope of the square of the photocurrent density curves, while the onset potential (V_{onset}) as shown in Figure 3 (c) was derived by taking the first derivative of the current density with respect to the applied potential.

The electrochemical impedance spectroscopy (EIS) measurements were performed using Autolab PGSTAT302N with the FRA module. The impedance spectra were recorded over a frequency range of 0.01 Hz to 1 MHz at ambient condition with an amplitude of 20 mV and under an applied potential of 0.23 V vs. Ag/AgCl (1.23 V_{RHE}) with one sun illumination.

The photo-generated gases and the Faradaic efficiency were measured using the gas tight three electrode PEC. The electrolyte filled gas-tight PEC was purged with argon gas for 3 hours before the PI-mode illumination to remove the dissolved O_2 from the electrolytes. The photogenerated gases were then collected from the headspace of the PEC and analysed using gas chromatography using a GC-8AIT gas chromatograph equipped with a TCD detector (Schimadzu Scientific Instruments, Columbia, USA).

S1.3 X-ray spectroscopy measurements

To investigate the stability of the α-Fe_2O_3 photo-anode and p-Si photocathode, X-ray absorption and emission spectroscopy (XAS-XES) was carried out on beamline ID-26 of the European synchrotron radiation facility (ESRF). A schematic view of the optics and the experimental set up is presented elsewhere[4, 5]. The incident X-ray energy was tuned at the Fe K-edge energy (for hematite photoanode) using a Si <311> double crystal monochromator and a Fe foil was used to calibrate the incident X-ray energy. Similarly, Ti K-edge energy (for p-Si photocathode) was tuned using a Si <111> double crystal monochromator and calibrated using a Ti foil. The size of the X-ray beam on the sample was 0.7 mm in horizontal and 0.1 mm in vertical directions. The high-energy resolution fluorescence detected X-ray absorption near edge structure (HERFD-XANES) spectra were recorded at the maximum of the Fe Kα1 and Ti Kα1 emission line. The fluorescence energy was selected by four Ge <333> (for hematite photoanode) and five Si <400> (for p-Si photocathode) bent crystal analysers arranged in Rowland geometry.[4, 6] and are detected on an avalanche photodiode. The samples were placed into a fluorescence geometry, such that the incident beam and the central crystal analyzer were at 45° with respect to the normal to the sample surface and a 90° angle between the incident beam and the central crystal analyser. All spectra shown in Figure S2 were normalized with respect to the total area.

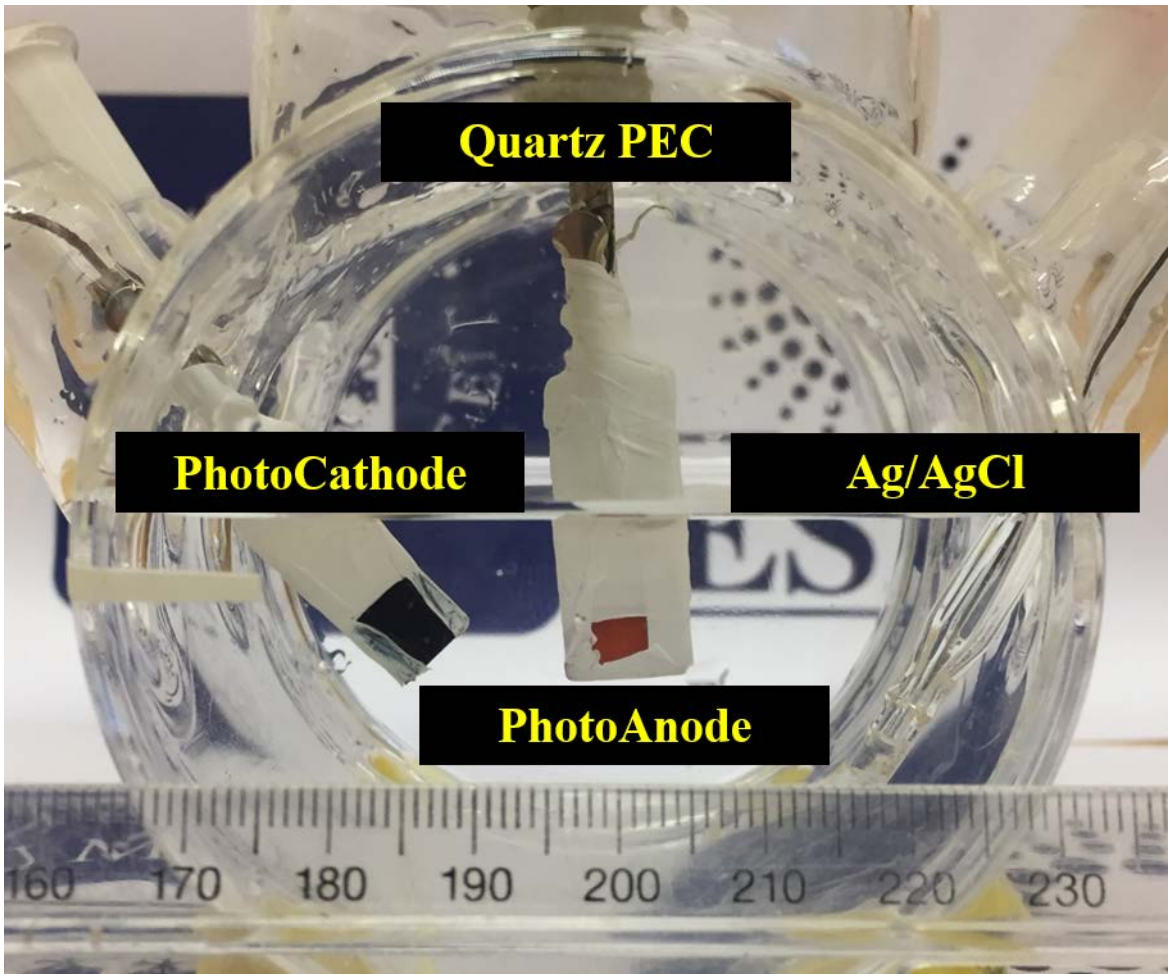

Figure S1: Digital photograph of the quartz photoelectrochemical cell (PEC) in parallel illumination mode showing FTO/ α-Fe_2O_3 photoanode as working electrode (center), p-Si /TiO_2/NiO_x as photocathode (left) and Ag/AgCl as reference electrode (right). The slightly larger area of counter electrode ensured better reaction kinetics at the working electrode[7].

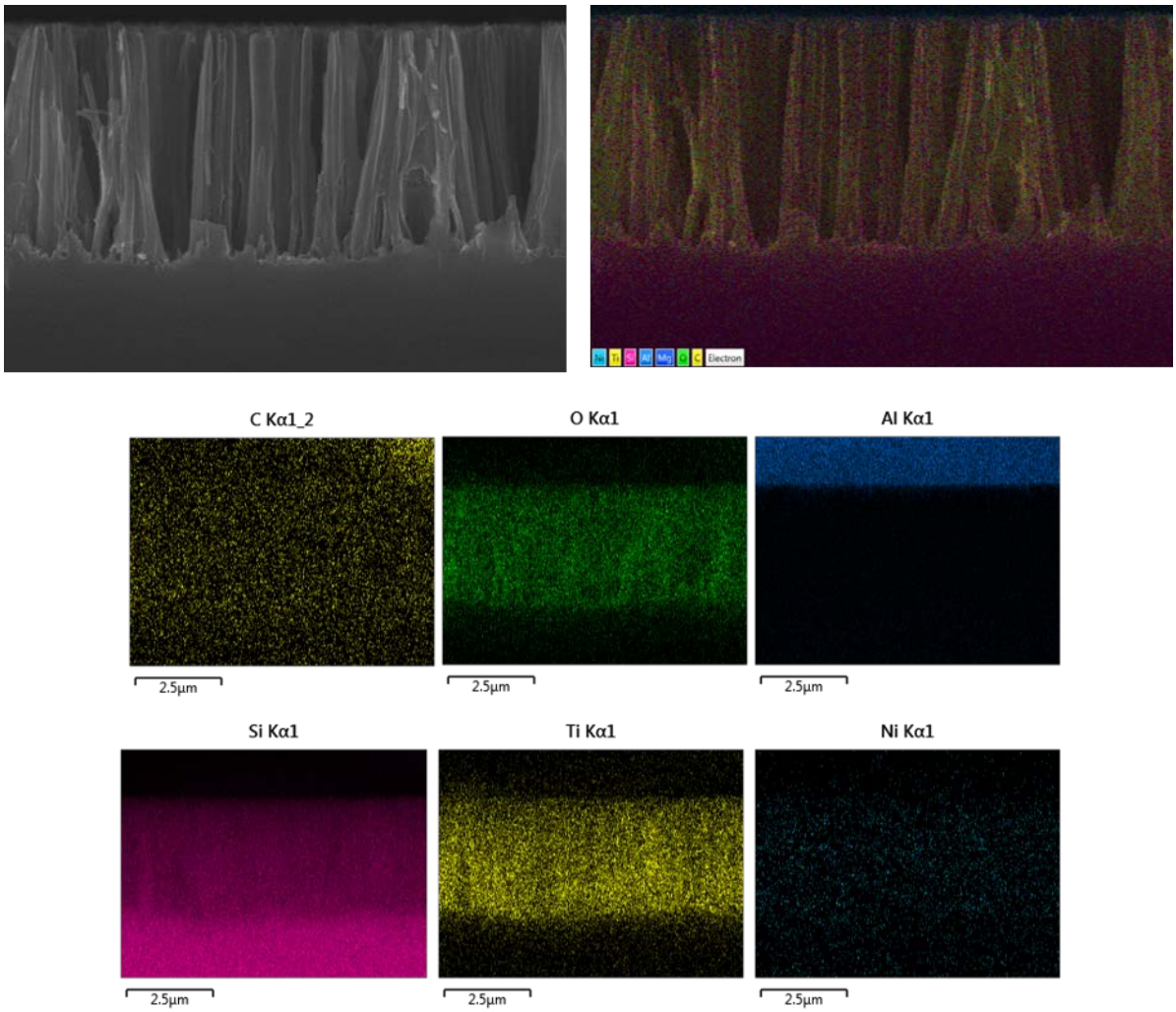

Figure S2: Morphological and elemental characterization of p-Si/TiO_2/NiO_x a) SEM image, b) EDX map of the selected area in the SEM image and c) distinct EDX maps indicating uniform distribution of TiO_2 and NiO_x on the Si MWs substrate.

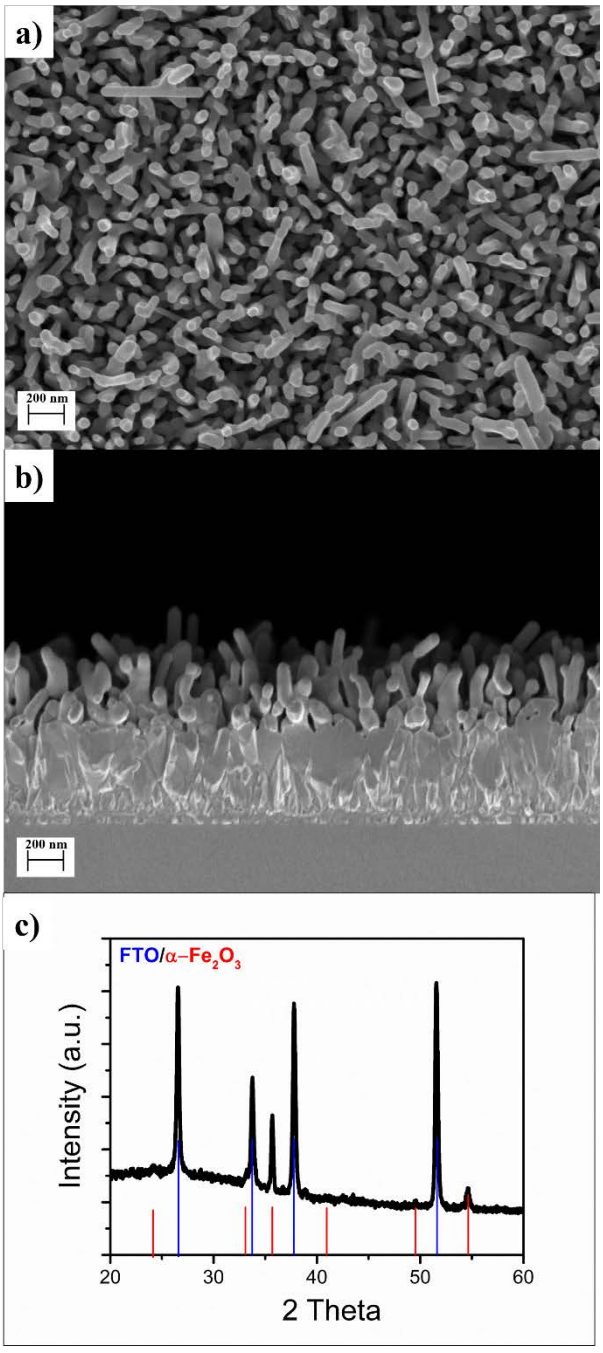

Figure S3: Morphological and elemental characterisation of α-Fe_2O_3 photoanode: a) planar and b) cross sectional SEM image. Panel c) shows an XRD pattern confirming the hematite phase.

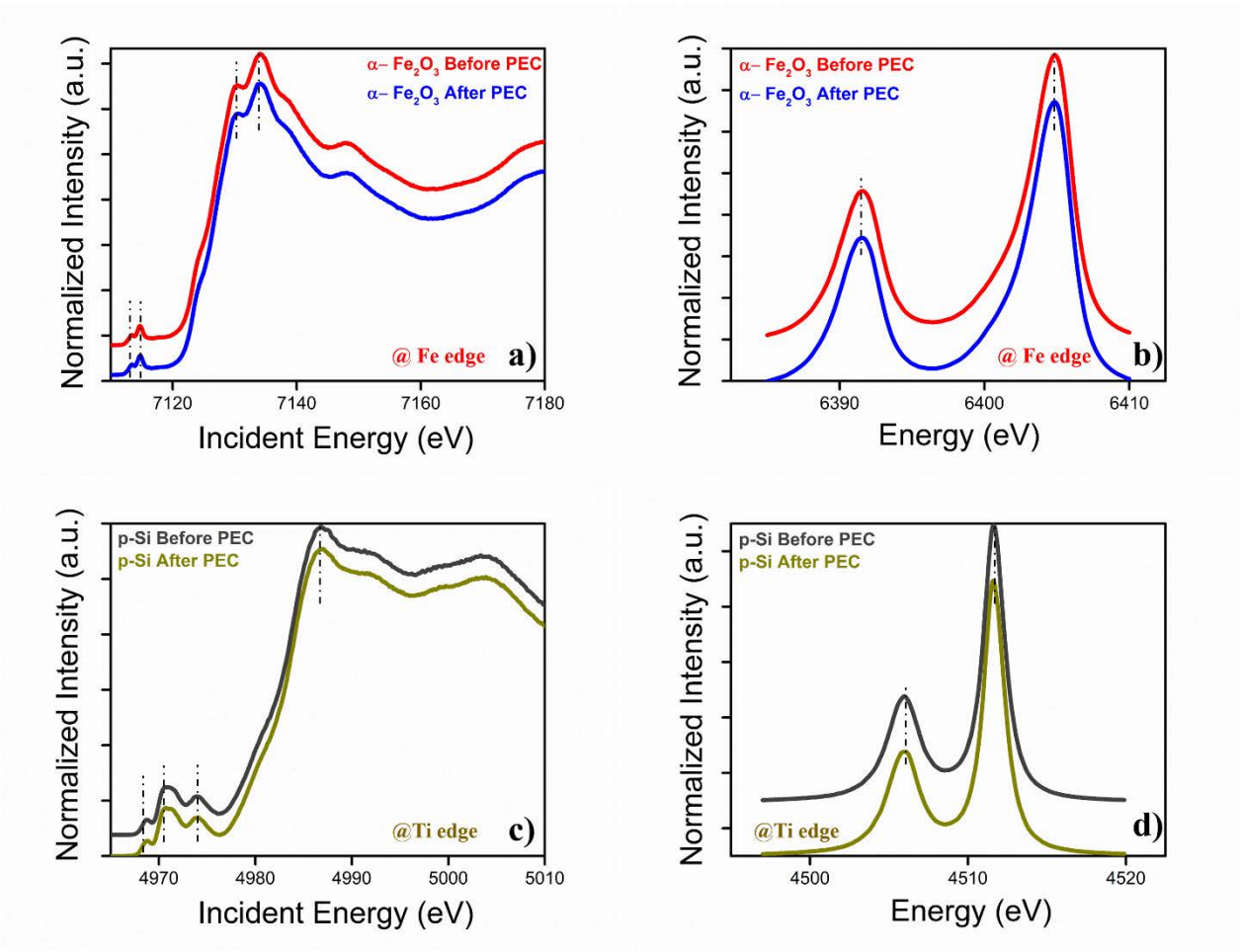

Figure S4: The electronic structure stability of the α-Fe_2O_3 photoanode and the p-Si/TiO_2/NiO_x (p-Si) photocathode as evident from the high-energy X-ray spectroscopy spectra of α-Fe_2O_3 and p-Si/TiO_2/NiO_x acquired at the Fe Kα1 and Ti Kα1 edges, respectively. The panels compare the spectra obtained before (red trace) and after (blue trace) the 6 hour photo-electrochemical water splitting experiment in parallel illumination mode. (a) and (c) HERFD-XANES acquired at Fe Kα1 and Ti Kα1, respectively. (b) and (d): X-ray emission spectra (XES) acquired at Fe Kα1 and Ti Kα1, respectively. In on our previous study[3], we observed that TiO_2 intermittent layer undergoes significant electronic and structural changes upon decoration with co-catalysts such as CoO_x or NiO_x that are critical for the performance. This is the primary reason to check the stability of p-Si/TiO_2/NiO_x photocathode at the Ti edge.

Table S1: Photoelectrochemical performances of semiconductor photoelectrode measured against expensive Pt as cathode or semiconductor photocathode

Photoanode	**Cathode$^{\Delta}$ Photocathode$^{\Delta\Delta}$**	**Illumination mode (pH)**	**J_{ph} (mA/cm^2)@1.23 V_{RHE} STH* ABPE** APCE*****	**Ref**
Pristine α-Fe_2O_3	p-Si/TiO_2/NiO_x $^{\Delta\Delta}$	Parallel (13.8)	1.26 0.14 **	**Our Work**
FTO/iron-oxide/NiFeOx (re-growth treatment)	a-Si/TiO_2/Pt$^{\Delta\Delta}$	Tandem (11.8)	~ 1.2 0.91*	[8]
Sb doped α-Fe_2O_3	Pt$^{\Delta}$	Single (13.8)	1.1 >0.1**	[9]
Co/APA/α-Fe_2O_3	Pt$^{\Delta}$	Single (13.8)	~ 1	[10]
F:SnO_2/WO_3/α-Fe_2O_3	Pt$^{\Delta}$	Single (13.6)	~ 1.7 8.0***	[11]

FTO/TiO_2/α-Fe_2O_3	Pt$^{\Delta}$	Single (13.6)	1.28	[12]
Co-Pi/$BiVO_4$	p-Cu_2O $^{\Delta\Delta}$	Tandem (6.0)	~ 3 0.5*	[13]
Co-Pi/Mo-$BiVO_4$	Pt/n/p- Si NWs $^{\Delta\Delta}$	Tandem (7.0)	0.57*	[14]
Co-Pi/$BiVO_4$	Zn-InP/TiO_2/Pt $^{\Delta\Delta}$	Parallel (7.0)	0.5*	[15]
$BiVO_4$/$NiFeO_x$	Pt/Mo/Ti/CdS/In_2S_3/($ZnSe_{0.85}CuIn_{0.7}Ga_{0.3}Se_2)_{0.15}$/Mo/SLG/Ti $^{\Delta\Delta}$	Parallel (9.2)	1.0*	[16]
FeOOH/Mo:$BiVO_4$/FTO	Ni/Si-cell/FTO $^{\Delta\Delta}$	Parallel (7.0)	2.5*	[17]

STH: solar to hydrogen efficiency
ABPE: applied bias photon to current efficiency
APCE: absorbed photon to current conversion efficiency

Table S2: EIS fitting parameters obtained for α-Fsse$_2$O$_3$ vs Pt or p-Si in the single illumination mode and in the parallel illumination mode in 1M NaOH (pH 13.8)

(R/Ω) **(CPE/F)**	**α-Fe_2O_3 vs Pt**	**α-Fe_2O_3 vs p-Si/TiO_2/NiO_x** **(SI-mode)**	**α-Fe_2O_3 p-Si/TiO_2/NiO_x** **(PI-mode)**
R_S	47	47	47
R_{CT1} **CPE_1**	42 8×10^{-6}	52 1×10^{-5}	64 1×10^{-5}
R_{CT2} **CPE_2**	439 2×10^{-5}	387 7×10^{-6}	298 3×10^{-6}

References

1. A. Annamalai, A. Subramanian, U. Kang, H. Park, S. H. Choi and J. S. Jang, *J. Phy. Chem. C*, 2015, **119**, 3810-3817.
2. K. Q. Peng, Y. J. Yan, S. P. Gao and J. Zhu, *Advanced Materials*, 2002, **14**, 1164-1167.
3. A. Kawde, A. Annamalai, L. Amidani, M. Boniolo, W. L. Kwong, A. Sellstedt, P. Glatzel, T. Wagberg and J. Messinger, *Sustainable Energy & Fuels*, 2018.
4. M. Rovezzi and P. Glatzel, *Semi. Sci. Tech.*, 2014, **29**, 023002.
5. L. Amidani, A. Naldoni, M. Malvestuto, M. Marelli, P. Glatzel, V. Dal Santo and F. Boscherini, *Angewandte Chemie International Edition*, 2015, **54**, 5413-5416.
6. P. Glatzel and U. Bergmann, *Coord. Chem. Rev.*, 2005, **249**, 65-95.
7. Z. Chen, T. F. Jaramillo, T. G. Deutsch, A. Kleiman-Shwarsctein, A. J. Forman, N. Gaillard, R. Garland, K. Takanabe, C. Heske and M. Sunkara, *J. Mater. Res.*, 2010, **25**, 3-16.
8. J.-W. Jang, C. Du, Y. Ye, Y. Lin, X. Yao, J. Thorne, E. Liu, G. McMahon, J. Zhu and A. Javey, *Nature communications*, 2015, **6**, 7447.
9. A. Annamalai, R. Sandström, E. Gracia-Espino, N. Boulanger, J.-F. Boily, I. Mühlbacher, A. Shchukarev and T. Wågberg, *ACS App. Mater. Inter.*, 2018, **10**, 16467-16473.
10. A. Y. Ahmed, M. G. Ahmed and T. A. Kandiel, *J. Phy. Chem. C*, 2016, **120**, 23415-23420.
11. K. Sivula, F. L. Formal and M. Gratzel, *Chem. Mater.*, 2009, **21**, 2862-2867.
12. A. Annamalai, P. S. Shinde, A. Subramanian, J. Y. Kim, J. H. Kim, S. H. Choi, J. S. Lee and J. S. Jang, *J. Mater. Chem. A*, 2015, **3**, 5007-5013.
13. P. Bornoz, F. F. Abdi, S. D. Tilley, B. Dam, R. Van De Krol, M. Graetzel and K. Sivula, *J. Phy. Chem. C*, 2014, **118**, 16959-16966.
14. P. Xu, J. Feng, T. Fang, X. Zhao, Z. Li and Z. Zou, *RSC Advances*, 2016, **6**, 9905-9910.
15. N. Kornienko, N. A. Gibson, H. Zhang, S. W. Eaton, Y. Yu, S. Aloni, S. R. Leone and P. Yang, *ACS Nano*, 2016, **10**, 5525-5535.
16. T. Higashi, H. Kaneko, T. Minegishi, H. Kobayashi, M. Zhong, Y. Kuang, T. Hisatomi, M. Katayama, T. Takata and H. Nishiyama, *Chem. Comm.*, 2017, **53**, 11674-11677.
17. C. Ding, W. Qin, N. Wang, G. Liu, Z. Wang, P. Yan, J. Shi and C. Li, *Phy.Chem.Chem.Phy.*, 2014, **16**, 15608-15614.